SCIENCE CHINA
Earth Sciences

SPECIAL TOPIC: Water in the Earth's interior
• REVIEW •

May 2016 Vol.59 No.5: 889–900
doi: 10.1007/s11430-016-5267-y

Electrical conductivity of hydrous silicate melts and aqueous fluids: Measurement and applications

GUO Xuan, CHEN Qi & NI HuaiWei*

CAS Key Laboratory of Crust-Mantle Materials and Environments, School of Earth and Space Sciences, University of Science and Technology of China, Hefei 230026, China

Received September 28, 2015; accepted January 12, 2016; published online February 2, 2016

Abstract The combination of magnetotelluric survey and laboratory measurements of electrical conductivity is a powerful approach for exploring the conditions of Earth's deep interior. Electrical conductivity of hydrous silicate melts and aqueous fluids is sensitive to composition, temperature, and pressure, making it useful for understanding partial melting and fluid activity at great depths. This study presents a review on the experimental studies of electrical conductivity of silicate melts and aqueous fluids, and introduces some important applications of experimental results. For silicate melts, electrical conductivity increases with increasing temperature but decreases with pressure. With a similar Na^+ concentration, along the calc-alkaline series electrical conductivity generally increases from basaltic to rhyolitic melt, accompanied by a decreasing activation enthalpy. Electrical conductivity of silicate melts is strongly enhanced with the incorporation of water due to promoted cation mobility. For aqueous fluids, research is focused on dilute electrolyte solutions. Electrical conductivity typically first increases and then decreases with increasing temperature, and increases with pressure before approaching a plateau value. The dissociation constant of electrolyte can be derived from conductivity data. To develop generally applicable quantitative models of electrical conductivity of melt/fluid addressing the dependences on temperature, pressure, and composition, it requires more electrical conductivity measurements of representative systems to be implemented in an extensive *P-T* range using up-to-date methods.

Keywords Silicate melts, Aqueous fluids, Electrical conductivity, Laboratory measurement, Partial melting

Citation: Guo X, Chen Q, Ni H W. 2016. Electrical conductivity of hydrous silicate melts and aqueous fluids: Measurement and applications. Science China Earth Sciences, 59: 889–900, doi: 10.1007/s11430-016-5267-y

1. Introduction

The solid earth contains a variety of silicate melts and aqueous fluids. They are crucial agents of transporting matter and energy in Earth's interior, and have played a key role in the geochemical cycling of elements including H and in the formation and evolution of the Earth. Many important geological phenomena and events, such as magma oceans, core-mantle differentiation, crust-mantle differentiation and volcanic eruptions, result from magmatism (Hofmann, 1988; Rubie et al., 2011; Elkins-Tanton, 2012; Coggon et al., 2013). Geological processes including plate tectonics and ore-forming processes are closely linked to aqueous fluids and silicate melts (Wyllie, 1988; Robb, 2005; Sigmundsson, 2006; Liebscher and Heinrich, 2007; Liebscher, 2010; Zheng and Herrmann, 2014; Barnes, 2015). Taking typical ocean-continent subduction zones as an example, the oceanic slab dehydrates in response to the change of temperature and pressure during subduction, and the released fluid metasomatizes the overlying mantle wedge and induces arc magmatism, ultimately leading to the formation of new con-

*Corresponding author (email: hwni@ustc.edu.cn)

tinental crust. This "subduction zone factory" has long been the focus of intensive studies on the solid Earth (Stern, 2002; Manning, 2004; Sun et al., 2014).

Silicate melts and aqueous fluids are electrically much more conductive than silicate minerals and rocks at the same temperature and pressure (Presnall et al., 1972; Gaillard, 2004; Ni et al., 2011a, 2011b, 2014; Yoshino and Katsura, 2013). Therefore, electrical conductivity anomalies in the deep Earth detected by magnetotelluric survey are often interpreted to indicate partial melting or fluid activity (Wei et al., 2001; Unsworth et al., 2005; Pommier, 2014). However, electrical conductivity of melts and fluids is controlled by temperature, pressure, and composition. In order to place more accurate quantitative constraints on the physicochemical status of the zones with conductivity anomaly, it is indispensable to carry out systematic laboratory measurements on the electrical conductivity of silicate melts and aqueous fluids with a variety of compositions across extensive temperature and pressure ranges. The combination of magnetotelluric survey and laboratory measurement of electrical conductivity has become a powerful approach for exploring the conditions and structure of Earth's deep interior (Yoshino et al., 2006; Karato and Wang, 2013; Naif et al., 2013; Pommier, 2014; McGary et al., 2014; Sifre et al., 2014). This paper presents a review on experimental studies of electrical conductivity of hydrous silicate melts and aqueous fluids, introduces some important applications with respect to probing partially molten zones, and finally discusses the outlook for future research.

2. Sample composition and preparation

Electrical conductivity measurements on hydrous silicate melts have been performed on compositions including rhyolite (Gaillard, 2004; Guo et al., 2016), dacite (Laumonier et al., 2015), phonotephrite (Pommier et al., 2008), basalt (Pommier et al., 2010a, 2010b; Ni et al., 2011b; Sifre et al., 2014), and albite (Ni et al., 2011a). The starting material is usually silicate glass with the designated composition. Nominal anhydrous glass (with <0.1 wt% H_2O) can be synthesized by mixing oxides and carbonates in proportions and fused at high temperature (CO_2 is expelled during the fusion). For rhyolite, natural obsidian can also be used as the starting material. Anhydrous glass powder and deionized water are sealed in a noble metal capsule and fused in a gas-medium high pressure vessel (either internal heated pressure vessel IHPV or external heated pressure vessel CSPV) or in a piston cylinder apparatus at constant temperature and pressure for a few days before being quenched to a hydrous glass. It requires the temperature to be above the liquidus and the system to be water-unsaturated. An ideal synthetic hydrous glass is transparent, homogeneous and free of bubble. To minimize sample deformation during electrical conductivity measurement, a single glass cylinder is preferred over compressed glass powder.

For aqueous fluids with more than 90 wt% of water, electrical conductivity studies focus on dilute solution of single electrolyte, such as NaCl (Quist and Marshall, 1968), KCl (Quist et al., 1970; Ho and Palmer, 1997), $CaCl_2$ (Frantz and Marshall, 1982), HCl (Frantz and Marshall, 1984), etc. These solutions can be prepared using traditional chemical methods.

3. Methods of electrical conductivity measurement

3.1 Methods for silicate melts

In the early days, electrical conductivity measurements on silicate melts employed a single-frequency alternating-current signal, usually performed at pressure <0.1 GPa (Presnall et al., 1972; Murase and Mcbimey, 1973; Waff and Weill, 1975; Rai and Manghnani, 1978; Satherley and Smedley, 1985). However, this method misses to capture the dependence of electrical conductivity on signal frequency (Huebner and Voigt, 1988; Huebner and Dillenburg, 1995; Karato and Wang, 2013). With the extensive use of sweeping-frequency impedance analyzer since the 1990s, the measurement precision has been improved significantly. The experimental temperature and pressure ranges are also expanded to up to 2173 K and 10 GPa (Gaillard, 2004; Pommier et al., 2008; Ni et al., 2011a, 2011b; Sifre et al., 2014, 2015; Laumonier et al., 2015).

Electrical conductivity measurements on hydrous silicate melts are quite challenging. Firstly, hydrous melts have low viscosity and can be easily deformed. Furthermore, they may dehydrate or may react with the capsule material, resulting in a change in composition. In addition, the measurement circuit is subject to short-circuit or to the disturbance from the heating loop due to the limited space in the high pressure apparatus. Building on the method of Gaillard (2004) in IHPV, Ni et al. (2011a, 2011b) designed a coaxial measurement circuit with an electromagnetic shielding in piston cylinder (Figure 1a). In this cell, the tube-like cylindrical sample is bracketed by a Pt rod as the inner electrode and a $Pt_{95}Rh_5$ capsule as the outer electrode, both connecting to a Solartron 1260 impedance analyzer by platinum wire. The assembly adopts insulating material such as Al_2O_3 and boron nitride (BN) as pressure media to reduce the background conductivity. A grounded molybdenum foil between the capsule and the graphite furnace serve to shield the measurement circuit from inductive effects of the heating loop. With this design, the geometry and composition of the melt remain largely intact after conductivity measurement, and the electromagnetic induction by the strong current in the heating loop is markedly suppressed. For this kind of two-electrode measurement, it is necessary to deduct the resistance of Pt lead wire from the measured resistance (Pommier et al., 2010b). The four-electrode method (Figure 1b)

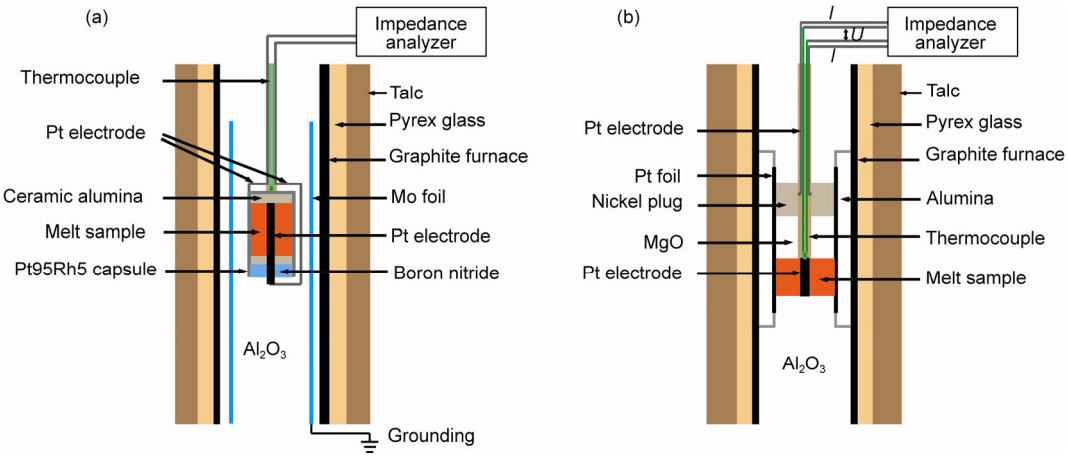

Figure 1 Sketches for electrical conductivity measurements on hydrous silicate melts in piston cylinder apparatus. (a) Two-electrode measurement (modified after Ni et al., 2011a); (b) four-electrode measurement (modified after Laumonier et al., 2015).

does not require resistance correction (Sifre et al., 2014; Laumonier et al., 2015), but the impedance spectra acquired are prone to severe disturbance from the heating loop in the absence of a shielding.

3.2 Methods for aqueous fluids

Even though electrical conductivity measurement of aqueous fluids was already accomplished at temperature up to 579 K and saturated vapor pressure as early as the beginning of the 20th century (Noyes, 1907), it took another half a century to extend the temperature and pressure range to the supercritical region (T>647 K, P>22 MPa). Using a coaxial cylindrical measurement circuit with Pt-Ir electrodes (Figure 2a), Fogo (1954) and Franck (1962) developed an excellent approach to measure electrical conductivity of aqueous solutions in CSPV at high temperature and pressure. With this method, the Oak Ridge National Laboratory of the United States determined electrical conductivity and dissociation constants of a variety of electrolytes such as NaCl up to 1073 K and 0.4 GPa (Quist and Marshall, 1968; Frantz and Marshall, 1982, 1984; Marshall and Frantz, 1987; Ho and Palmer, 1997). The upper bound of pressure is restricted to 0.4 GPa, corresponding to <15 km depth, due to limitation on the tensile strength of the vessel material (Ni alloy). Electrical conductivity measurements on fluids were performed in China at pressure up to 5 GPa (Xu et al., 1997; Su et al., 2000), but the temperature was limited to 773 K and the reliability of that approach requires more rigorous assessment. Therefore, the above two methods are inadequate for the high T-P conditions in Earth's deep interior, such as in the mantle wedge in subduction zones.

Recently, Ni et al. (2014) developed a new technique to measure electrical conductivity of fluids in a modified Bassett type hydrothermal diamond anvil cell (HDAC, Figure 2(b)). This approach has the potential to reach 1173 K and 4 GPa. They installed a laser-perforated diamond disk between the two diamond anvils of a regular HDAC. Two Ir

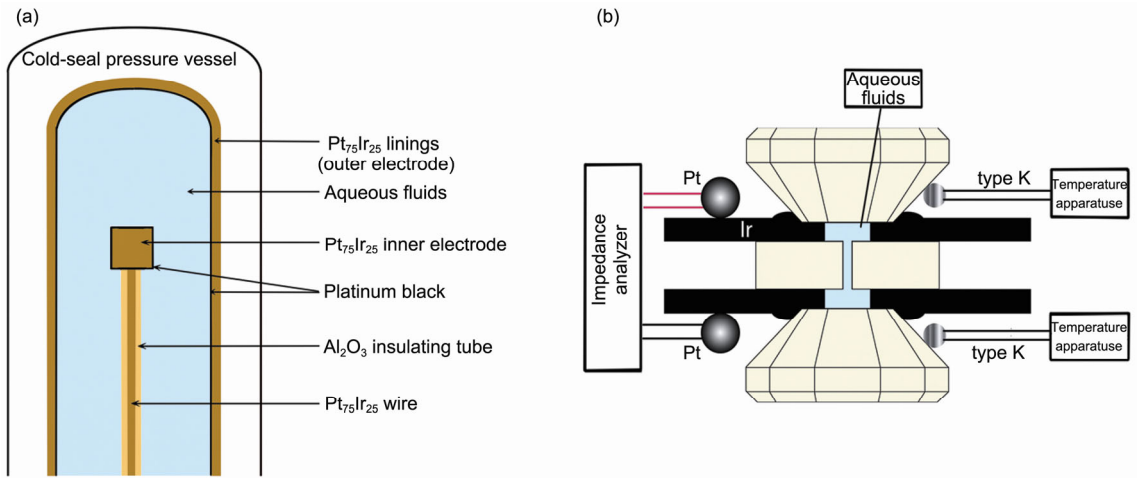

Figure 2 Sketches for electrical conductivity measurements on aqueous fluids. (a) In cold-seal pressure vessel (modified after Marshall and Frantz, 1987); (b) in hydrothermal diamond anvil cell (modified after Ni et al., 2014).

gaskets were bracketed between the three diamond pieces, serving as both sample chambers and electrodes, and four Pt wires connected the Ir electrodes to a Solartron 1260 impedance analyzer. Resistance loop of molybdenum wires provided external heating, with temperature being monitored by two K-type thermocouples. Because the sample chamber was approximately isochoric during the heating and cooling processes, pressure can be calculated from the equation of state of pure water (Wagner and Pruss, 2002).

3.3 Calculation of resistance and electrical conductivity

The direct-circuit resistance of the sample can be extracted from interpreting the impedance spectrum (Huebner and Dillenburg, 1995). The conductivity cell constant (in m^{-1}) is also required to calculate the electrical conductivity of silicate melts or aqueous fluids. For silicate melts, the cell constant can be derived from the geometry parameters of the sample. For aqueous fluids, the cell constant is calibrated using the certified electrical conductivity of a standard solution at ambient conditions (Marshall and Frantz, 1987; Ni et al., 2014). Taking the electrical conductivity measurement of KCl solution in HDAC as an example, the cell constant is the product of the resistance measured at ambient conditions and the corresponding conductivity value in literature, with ~1% error. The product of the cell constant and the fluid conductance (the reciprocal of resistance, with ~6% error) measured at high *T*-*P* then yields the electrical conductivity of the solution. The overall uncertainty of fluid conductivity measurement in HDAC is estimated to be less than 10% (Ni et al., 2014).

4. Data and models

As ionic conductors, electrical conductivity of silicate melts and aqueous fluids is controlled by the concentration and mobility of ions, which in turn depend on physicochemical conditions.

4.1 Hydrous silicate melts

Literature experimental studies on electrical conductivity of silicate melts are summarized in Table 1. Below, we present a detailed analysis about the effects of temperature, pressure, oxygen fugacity, melt composition and water content on electrical conductivity.

4.1.1 Temperature effect

Electrical conductivity of silicate melts increase with increasing temperature. Generally, the variation of electrical conductivity (σ) with temperature (T) can be described by

Table 1 A list of experimental studies on electrical conductivity of silicate melts

Experimental system	T (K)	P (GPa)	H_2O (wt%)	SiO_2 (wt%)	Na_2O (wt%)	H_a (kJ/mol)	ΔV_a (cm^3/mol)	Method (two/four-electrode)	Data sources
Phonolite	352–1306	0–0.4	0–5.6	55.73	6.11	61–107	18–22	2	Pommier et al., 2008
Phonotephrite	399–1325	0–0.4	0–3.5	48.54	3.54	92–129	20–24	2	Pommier et al., 2008
Tephrite	719–1575	0–0.4	–	49.24	1.97	80–142	16–22	2	Pommier et al., 2008
	1473–1673	0–1.7	–	51.20	2.48	120–131	–0.1–4.6	2	Tyburczy and Waff, 1983
	1473–1596	0	–	54.81	3.62	109	–	2	Gaillard and Iacono-Marziano, 2005
Basalt	1473–1673	0	–	50.00	2.29	112–114	–	2	Pommier, 2010a
	1573	0	–	49.60	2.29	177	–	2, 4	Pommier, 2010b
	1473–1923	2.0	0–6.3	50.06	3.67	53–142	–	2	Ni et al., 2011b
Andesite	1473–1673	0–2.5	–	62.04	5.01	72–142	3.3–17.9	2	Tyburczy and Waff, 1983
	1431–1596	0	–	59.60	4.01	86		2	Gaillard and Iacono-Marziano, 2005
	1473–1673	0–2.5	–	68.00	4.59	60–89	5.3–11.1	2	Tyburczy and Waff, 1985
Dacite	1361–1596	0	–	65.38	4.10	72	–	2	Gaillard and Iacono-Marziano, 2005
	673–1623	0.1–3.0	0–11.8	67.93	2.09	62–96	4.0–25	4	Laumonier et al., 2015
	1473–1673	0–2.5	–	78.07	3.80	46–82	3.2–7.9	2	Tyburczy and Waff, 1985
Rhyolite	623–1598	0.05–0.4	0–3.0	74.51	4.15	61–70	20	2	Gaillard, 2004
	678–1665	0.5–1.0	0.1–7.9	75.72	4.68	36–68	7.8–18.1	2	Guo et al., 2016
Albite melt	777–1060	0–6.0	–	67.76	12.09	55–90	–	2	Bagdassarov et al., 2004
	473–2173	0.9–10.0	0–5.7	68.90	11.30	47–95	3.7–23	2	Ni et al., 2011a

the Arrhenius equation:

$$\sigma = \sigma_0 \exp\left(-\frac{H_a}{RT}\right), \quad (1)$$

where σ_0 is the pre-exponential factor, H_a is the activation enthalpy, R is the gas constant. Eq. (1) implies that logarithmic electrical conductivity is linearly correlated with reciprocal temperature (Figure 3a, b). This is usually valid only within the liquid region or within the glass region separately, but in some cases such as in rhyolitic melts (Gaillard, 2004; Guo et al., 2016), H_a does not change notably even across the glass transition. For anhydrous melts, an inflection point near the glass transition temperature often appears on the logσ versus 1/T curve, with the activation enthalpy being higher in the liquid region (Bagdassarov et al., 2004; Pommier et al., 2008; Ni et al., 2011a). For hydrous melts, the transition from the glass to the liquid region is gentler, with a lower H_a in the liquid region (Pommier et al., 2008; Ni et al., 2011a). The behavior of hydrous melts is more consistent with the prediction of the relaxation theory of melt structure (Dingwell and Webb, 1990; Ni et al., 2015). Basaltic liquids even show deviation from the Arrhenius law in a narrow temperature range, yielding a concave logσ-1/T curve (Figure 3c) (Waff and Weill, 1975; Tyburczy and Waff, 1983; Ni et al., 2011b). In contrast, a convex logσ-1/T curve is found for albite liquid at 10 GPa (Ni et al., 2011a).

4.1.2 *Pressure effect*

The Arrhenius equation can also incorporate the change of electrical conductivity with pressure (P):

$$\sigma = \sigma_0 \exp\left(-\frac{E_a + P\Delta V_a}{RT}\right), \quad (2)$$

where E_a and ΔV_a are the activation energy and the activation volume, respectively. In contrast to the temperature effect, pressure has a negative impact on the electrical conductivity of silicate melts, being more pronounced at low temperature. If ions and atoms are regarded as incompressible hard balls, the "free volume" (the volume not occupied by ions and atoms) in melt structure shrinks upon compression. This mechanism may explain the decline of ion mobility and of electrical conductivity. The negative influence of pressure on electrical conductivity yields positive activation volumes (ΔV_a), which typically range from 3 cm^3/mol to 30 cm^3/mol (Table 1) and tend to decrease with pressure (Tyburczy and Waff, 1983, 1985).

4.1.3 *Effect of oxygen fugacity*

Experiments on iron-bearing basaltic and andesitic melts indicate that electrical conductivity is insensitive to oxygen fugacity (Waff and Weill, 1975; Pommier et al., 2010a). For basaltic melt, a change in oxygen fugacity over 8 orders of magnitude results in only a variation of 0.2 log unit in electrical conductivity (Pommier et al., 2010a). Therefore, the effect of oxygen fugacity can generally be ignored.

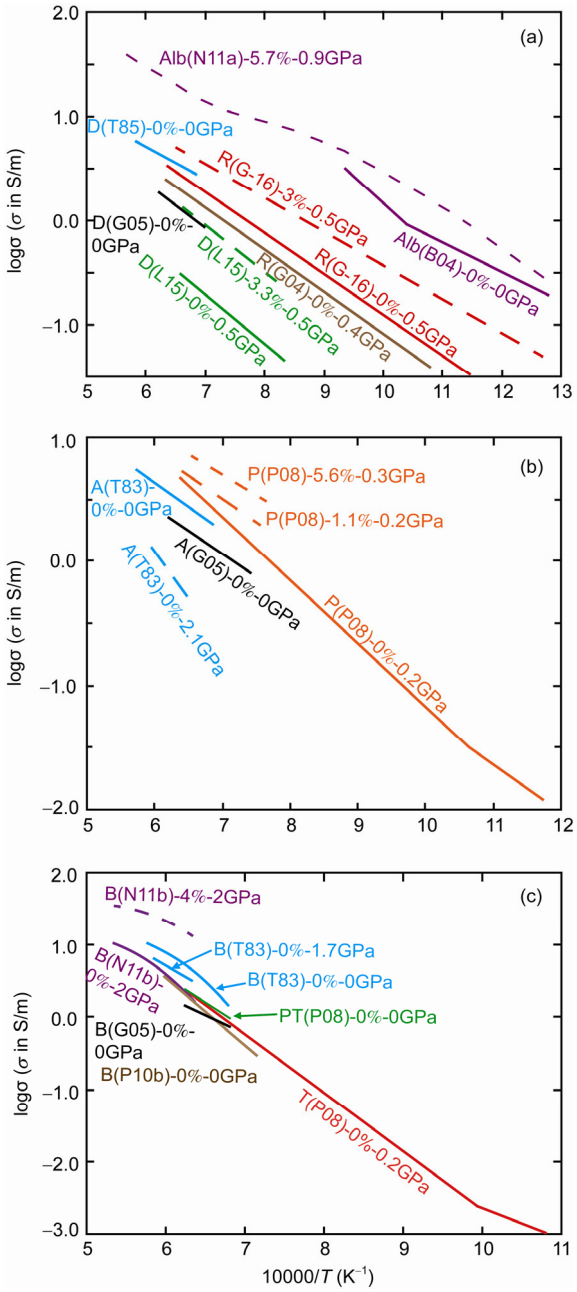

Figure 3 Electrical conductivity of silicate melts with various compositions. (a) Felsic melts; (b) intermediate melts; (c) mafic melts. The solid and dashed curves are for anhydrous and hydrous melts, respectively, with the labels indicating the weight percentage of water and pressure. Alb, albite; D, dacite; R, rhyolite; A, andesite; B, basalt; P, phonolite; PT, phonotephrite; T, tephrite. Data sources: Tyburczy and Waff (1983, 1985), Gaillard (2004), Bagdassarov et al. (2004), Gaillard and Iacono-Marziano (2005), Pommier et al. (2008), Pommmier et al. (2010a), Ni et al. (2011a, 2011b), Laumonier et al. (2015), Guo et al. (2016).

4.1.4 *Dependence on melt composition*

Electrical conductivity of silicate melts is strongly controlled by melt composition, in particular the content of SiO_2, Na_2O,

and H_2O. Because Na^+ travels much faster than other major elements (especially in polymerized melts), the concentration and mobility of Na^+ often dominate electrical conduction. With similar SiO_2 content or degree of polymerization, the melt with more Na_2O yields higher electrical conductivity. For example, the disparities between different studies on dacitic melt (Figure 3(a)) result primarily from the difference in Na_2O concentration. When Na_2O content is comparable, electrical conductivity for anhydrous melts along the calc-alkaline series generally follow the trend basalt<andesite<dacite<rhyolite (Tyburczy and Waff, 1983, 1985; Gaillard, 2004; Gaillard and Iacono-Marziano, 2005), which is consistent with the increasing trend of Na^+ diffusivity from basalt to rhyolite (Lowry et al., 1982; Henderson et al., 1985). The activation enthalpy of electrical conductivity increases from 36–87 kJ/mol in rhyolitic, to 62–96 kJ/mol in dacitic, to 72–113 kJ/mol in andesitic, and to 53–142 kJ/mol in basaltic melts. This probably implies an increasing contribution of network modifying cations other than Na^+ (Ni et al., 2015). Similar activation volumes are obtained for anhydrous silicate melt with different composition. As for hydrous melts, ΔV_a for dacitic melt increases with increasing water content (Laumonier et al., 2015), but rhyolitic melt shows the opposite trend (Guo et al., 2016).

The incorporation of water reduces the activation enthalpy and enhances electrical conductivity of silicate melts (Figure 4). Guo et al. (2016) found that the effect of water on electrical conductivity of rhyolitic melt was significantly underestimated in a previous study (Gaillard, 2004). The positive effect by water is more pronounced for basaltic melt than for felsic melts (Ni et al., 2011b). This likely reflects that the mobility of Ca^{2+} and Mg^{2+}, which contribute to electrical conduction in basaltic melt, is promoted more effectively by hydration than H_2O does for Na^+, the predominant charge carrier in rhyolitic melt. It is generally accepted that hydrous species such as proton and hydroxyl (OH^-) do not play a significant role in electric conduction (Gaillard, 2004; Ni et al., 2011a, 2015; Laumonier et al., 2015).

CO_2 solubility in silicate melts is much lower than water solubility (Blank, 1993; Ni and Keppler, 2013). The influence of CO_2 on electrical conductivity is also weaker. When CO_2 concentration is below 0.5 wt%, electrical conductivity of basaltic melt shows little change (Ni et al., 2011b). However, when CO_2 is more than 10 wt%, it enhances electrical conductivity of basaltic melt significantly, which may reflect a combination effect of mobilizing the existing cations and the ionic transport of CO_3^{2-} itself.

4.1.5 Electrical conductivity models

Electrical conductivity models accounting for the dependences on temperature, pressure and water content have been developed for specific melt compositions, such as for albite and rhyolite (Ni et al., 2011a; Guo et al., 2016). Some authors have also attempted to incorporate melt composition and to develop a widely applicable electrical conductivity model (Poe et al., 2008; Pommier and Le-Trong, 2011). However, there are often substantial differences between experimental data and model predictions (Laumonier et al., 2015). To establish a generally applicable model with high precision, it requires both the accumulation of more experimental data covering a variety of compositions and more in-depth understanding of the physical mechanisms for electrical conduction.

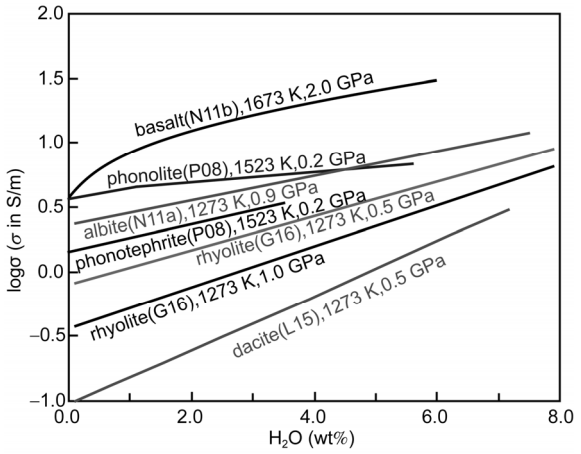

Figure 4 Electrical conductivity of silicate melts as a function of H_2O concentration. Data are from Pommier et al. (2008); Ni et al. (2011a, 2011b); Laumonier et al. (2015); Guo et al. (2016).

4.1.6 The relationship between electrical conductivity and ion diffusivity

Both electrical conductivity and diffusivity are transport properties of silicate melts and are closely coupled with the motion of ions. When electrical conductivity is dominated by a single ionic species with the highest mobility, such as Na^+, electrical conductivity can be related to the diffusivity (D) of that species via the Nernst-Einstein equation:

$$\sigma_i = \frac{1}{H_R}\frac{Dc(zF)^2}{RT}, \tag{3}$$

where c and z are the concentration (in mol/m^3) and valence of the ion, F is the Faraday constant, and H_R is the Haven ratio depending on the transport mechanism (being 1 for an interstitial motion in silicate melts). Experimental values of electrical conductivity and Na^+ diffusivity in silicate melts are generally consistent with the Nernst-Einstein equation (Figure 5), supporting the dominant role of Na^+ in electrical conduction.

4.2 Electrical conductivity of aqueous fluids and dissociation constant

Electrical conductivity studies for aqueous fluids mainly focused on dilute solutions of a single electrolyte (e.g. salt, acid, or base) (Table 2). Experiments were mostly performed

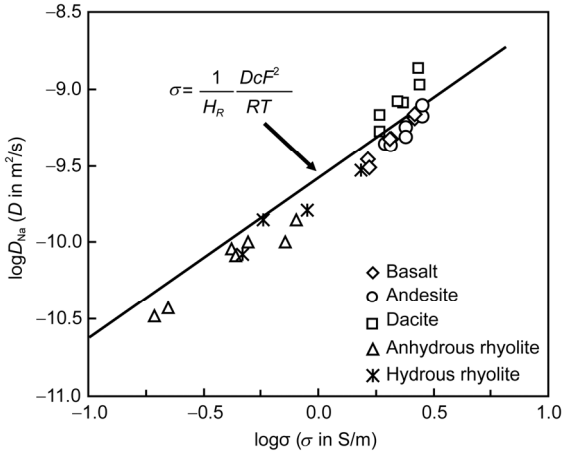

Figure 5 Electrical conductivity and Na^+ diffusivity roughly conform to the Nernst-Einstein equation. The solid line represents the Nernst-Einstein equation for a Na_2O content of 4.7 wt%. Sources for Na^+ diffusivities of Na^+: Lowry et al. (1982) (basalt and andesite), Henderson et al. (1985) (dacite); Jambon (1982) (anhydrous rhyolite); Watson (1981) (hydrous rhyolite). Electrical conductivities are from Gaillard (2004) and Gaillard and Iacono-Marziano (2005).

at temperatures <1073 K and pressures <0.4 GPa. For a specific electrolyte, its dissociation constant can be derived from electrical conductivity measurements of a series of solutions with different concentrations.

4.2.1 Temperature and pressure effects

NaCl solutions are taken as an example in the following discussion. Upon heating at constant pressure, a NaCl solution with a specific molality shows a marked increase in electrical conductivity until temperature approaches 573–673 K, which is followed by a conductivity decrease toward higher temperature (Figure 6a). This trend can be understood by considering the mobility and concentration of ions, which are in turn closely related to the physicochemical properties of water including density, viscosity and dielectric constant (Figure 7). At the beginning of heating, viscosity of water decreases rapidly and the mobility of ions in the solution is remarkably strengthened, leading to an increase in electrical conductivity. However, because pressure is fixed, the density of the solution decreases with increasing temperature, resulting in a decrease in the molarity of electrolyte. More importantly, the dielectric constant of water is dramatically reduced when temperature surpasses 573–673 K, and the suppressed ionization leads to a rapid drop in the concentration of Na^+ and Cl^- and in electrical conductivity (Quist and Marshall, 1968). Other electrolytes such as KCl and CsCl show similar behavior (Quist and Marshall, 1969).

Table 2 Experimental studies of electrical conductivity on aqueous solutions

Experimental system	Temperature range (K)	Pressure range (GPa)	Data source
NaCl	579	Saturated vapor pressure	Noyes, 1907
	666	0.30	Fogo et al., 1954
	1023	0.25	Franck, 1956
	1073	0.40	Quist and Marshall, 1968, 1969
	673	0.28	Zimmerman et al., 1995
	773	5.00	Xu et al., 1997
	773	4.00	Zheng et al., 1997
KCl	579	Saturated vapor pressure	Noyes, 1907
	1023	0.25	Franck, 1956
	1023	1.20	Quist et al., 1970
	873	0.30	Ho and Palmer, 1997
	773	1.20	Su et al., 2000
	973	0.76	Ni et al., 2014
$CaCl_2$, $MgCl_2$	973	0.40	Frantz and Marshall, 1982
HCl	579	Saturated vapor pressure	Noyes, 1907
	1023	0.25	Franck, 1956
	973	0.40	Frantz and Marshall, 1984
NaOH, KOH	579	Saturated vapor pressure	Noyes, 1907
	1023	0.25	Franck, 1956
	873	0.30	Ho and Palmer, 1997
Na_2SO_4, K_2SO_4	579	Saturated vapor pressure	Noyes, 1907
	1073	0.40	Quist and Marshall, 1968, 1969
	673	0.03	Sharygin et al., 2006

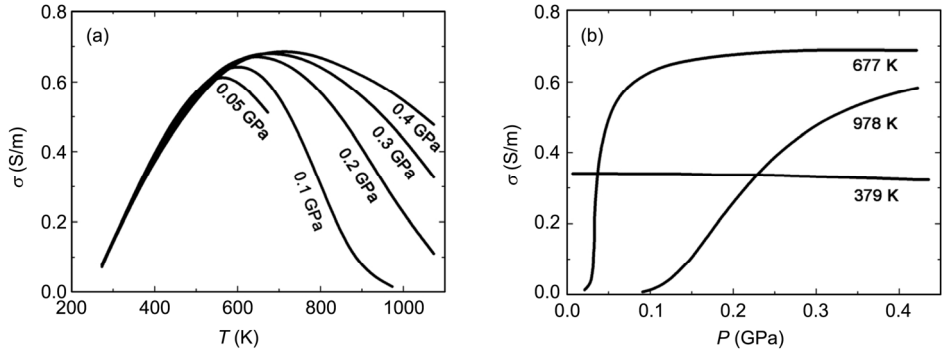

Figure 6 Electrical conductivity of NaCl solution (0.01 mol/kg) as a function of temperature and pressure. Modified after Quist and Marshall (1968).

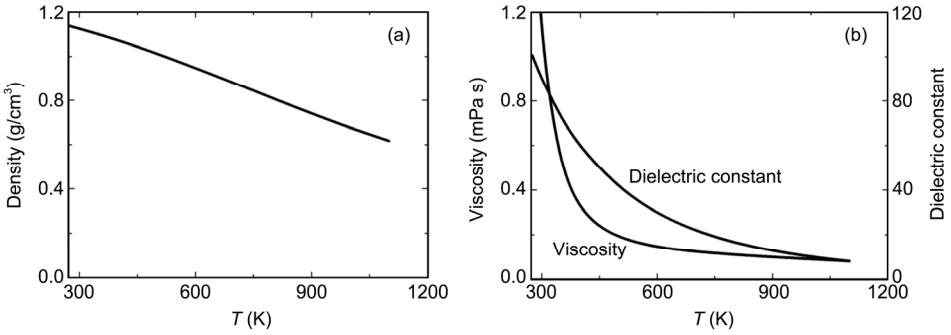

Figure 7 Density, viscosity and dielectric constant of water as a function of temperature. Modified after Quist and Marshall (1968).

Electrical conductivity of NaCl solution shows contrasting variation with pressure at different temperatures (Figure 6b). At low temperature (e.g., 379 K), NaCl as a strong electrolyte is almost fully ionized. Compression has limited impact on the density of the solution and on the concentration of ions, leading to a minimal change in electrical conductivity. But at 677 K, electrical conductivity increases rapidly with pressure before reaching a plateau at ~0.2 GPa, as a result of increasing molarity and increasing degree of ionic dissociation, which are in turn due to the increase in density and in dielectric constant. The higher the temperature, the more "room" for ion concentration to increase, the broader pressure range in which electrical conductivity can maintain the increasing trend.

4.2.2 Dissociation constant and limiting molar conductivity

Electrical conductivity is controlled by the concentration of electrolyte to a great extent. Dissociation constant and molar conductivity (electrical conductivity normalized by molarity) better characterize how strong the electrolyte is. For the dissociation reaction of NaCl solution:

$$\mathrm{NaCl}_{(aq)} \Leftrightarrow \mathrm{Na}^{+}_{(aq)} + \mathrm{Cl}^{-}_{(aq)}, \tag{4}$$

the dissociation constant of NaCl is given to be

$$K = \frac{a_{\mathrm{Na}^+} a_{\mathrm{Cl}^-}}{a_{\mathrm{NaCl}}}, \tag{5}$$

where a is the activity of an ion or an associated ion pair. Because the activity coefficient of the ion pair NaCl is usually assumed to be 1, eq. (5) becomes

$$K = \frac{a_{\mathrm{Na}^+} a_{\mathrm{Cl}^-}}{[\mathrm{NaCl}]} = \frac{[\mathrm{Na}^+][\mathrm{Cl}^-]\gamma_{\pm}^2}{[\mathrm{NaCl}]} = \frac{\alpha^2 M \gamma_{\pm}^2}{(1-\alpha)}, \tag{6}$$

where the square brackets denote molar concentration, M is the molarity of the solution, $\gamma_{\pm}$ is the mean activity coefficient of the ions, and α is the degree of dissociation. Dissociation constant and limiting molar conductivity (the molar conductivity toward nil concentration) at a given P-T condition can be obtained by measuring electrical conductivity of a series of solutions with different concentrations, followed by fitting the data set of molar conductivity versus molar concentration using the Ostwald's dilution law or more sophisticated models (e.g., the Shedlovsky equation, Fuoss and Shedlovsky, 1949). Many studies find a good linear correlation between limiting molar conductivity and fluid density at temperatures above 673 K, and this correlation shows little change upon further increase in temperature (Marshall and Frantz, 1987).

Dissociation constant generally decreases with increasing temperature but increases with pressure (Figure 8). This is again consistent with the change of dielectric constant with temperature and pressure. The newly developed technique for electrical conductivity measurement (Ni et al., 2014) allows to acquire the dissociation constants at conditions corresponding to subduction zone depths, but more systematic

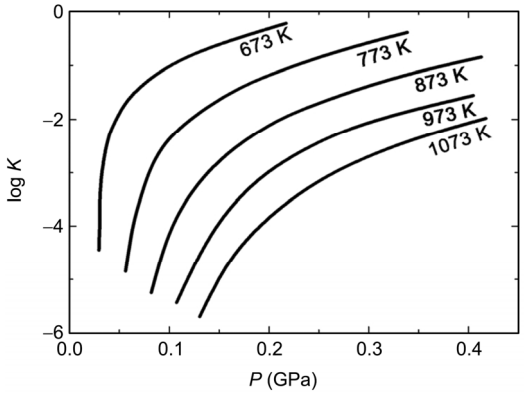

Figure 8 Dissociation constant of KCl solution as a function of temperature and pressure (modified after Quist and Marshall, 1968).

measurements await to be carried out.

5. Applications

5.1 The conductivity anomaly at the oceanic lithosphere-asthenosphere boundary

At a few hundred kilometers away from the mid-ocean ridge, magnetotelluric survey identified conductivity anomaly as high as 0.1 S/m and strong anisotropy, with conductivity being the highest in the direction of plate spreading, at 60–130 km depths in the mantle (Evans et al., 2005). This depth range roughly corresponds to the lithosphere-asthenosphere boundary and also to the seismic low-velocity zone (Dziewonski and Anderson, 1981). This coupling of low velocity and high conductivity is widely believed to indicate the presence of a small amount of silicate melt (Anderson and Sammis, 1970; Yoshino et al., 2006). However, experimental electrical conductivity of anhydrous basaltic melt requires at least 5–10 vol% melt to match the observed bulk conductivity (Tyburczy and Waff, 1983), posing a significant challenge to this interpretation. Such high melt fraction would result in gravitational segregation (Faul, 2001), prohibiting a long-term stable presence of the melt. Ni et al. (2011b) find that water significantly enhances the electrical conductivity of basaltic melt. During mantle melting, water as a highly incompatible component preferentially joins the melt phase. For a depleted mantle with 125 ppm H_2O, 1–2% hydrous melt is sufficient to match the observed conductivity anomaly, and it requires only 0.2–0.5% melt for an enriched mantle with 600 ppm H_2O. Accordingly, Ni et al. (2011b) suggest that the low-velocity and high-conductivity layer at the oceanic lithosphere-asthenosphere boundary may contain a small amount of hydrous basaltic melt segregating into tube-like structure, elongated in the direction of plate spreading. Sifre et al. (2014) further show that even smaller melt fraction and lower temperature are required if the effect of CO_2 on electrical conductivity of the melt is taken into account, which provides an explanation for electrical conductivity anomaly in the asthenosphere beneath older oceanic plates.

5.2 Crustal conductivity anomaly in the Himalaya-Tibet orogen

The Himalayan-Tibetan orogenic belt represents a typical case of continental collision (Yin and Harrison, 2000; Royden et al., 2008; Xu et al., 2006). Geophysical surveys detected a low-velocity and high-conductivity zone in the crust of Himalaya and Southern Tibet (Van Ngoc et al., 1986; Chen et al., 1996; Wei et al., 2001; Li et al., 2003; Gaillard, 2004; Unsworth et al., 2005; Caldwell et al., 2009). In particular, the INDEPTH MT team located conductive layers at 30–50 km depths (with a bulk conductivity up to 0.3 S/m) in the southern Tibet, and at 20–40 km depths in the northwestern Himalaya (with a bulk conductivity up to 0.1 S/m) (Wei et al., 2001; Unsworth et al., 2005). Some workers suggested that the low-velocity and high-conductivity phenomenon could be caused by water-rich or Fe^{3+}-rich pyroxene and plagioclase (Yang et al., 2011) or thin layers of fluid (e.g., Makovsky and Klemperer, 1999). Others consider silicate melt to be more plausible based on the evidences from the low seismic velocity, strong *P*-to-*S* wave conversion, high heat flow, and high conductivity (Kind et al., 1996; Francheteau et al., 1984; Chen et al., 1996; Unsworth et al., 2005). Experimental petrology studies indicate that the muscovite-bearing metapelite in this region undergo dehydration melting at temperature above 923 K, and the produced hydrous rhyolitic melt has a composition similar to the Miocene leucogranite in the Himalayan-Tibetan orogenic belt (Harris et al., 1995; Law et al., 2004; Searle et al., 2006; Hashim et al., 2013). By assuming electrical conductivity of the melt to be 3–10 S/m, Unsworth et al. (2005) inferred that a melt fraction of 5–14% and 2–4% would match the observed electrical conductivity at South Tibet and Northwest Himalaya, respectively. In contrast, electrical conductivity measurement of partially molten metapelite reveals that it requires 100 vol% and 25 vol% melt, respectively, to reach the geophysical observation (Hashim et al., 2013). Such high amounts of silicate melts are unrealistic in the lower crust, which probably arises from an underestimation of the elevating effect of water on melt conductivity (Guo et al., 2016)

6. Summary and prospects

Experimental studies on electrical conductivity of silicate melts and aqueous fluid have made considerable progress over the past decades, played an important role in understanding the conditions of Earth's interior, and promoted understanding of the microscopic structure of silicate melts and aqueous fluids. Natural silicate melts are compositionally diverse, and the compositions covered by experimental stud-

ies are still limited. For example, to date electrical conductivity of hydrous andesitic melts has not been investigated at all. Therefore, electrical conductivity measurements of more silicate melts across an extensive range of temperature and pressure are welcome. Such effort is required to develop a generally applicable quantitative electrical conductivity model for silicate melts, which will provide a solid foundation for probing molten zones in Earth's interior. Most electrical conductivity measurements of aqueous fluids are still restricted to simple electrolyte solutions at high-T and low-P, or low-T and high-P conditions. Our understanding of the ionization behavior of fluids at great depths in subduction zones is still inadequate. With the emergence of new experimental techniques, major breakthroughs in quantification of electrical conductivity of aqueous fluids at high-T and high-P conditions are likely to be made in the near future. Furthermore, it may even be possible to measure the electrical conductivity of supercritical fluids with an intermediate composition relative to silicate melts and aqueous fluids, which will provide a crucial clue for understanding the activity of supercritical fluids in subduction zones.

Acknowledgements *We thank Editor Yongfei Zheng for invitation to contribute. Comments from Prof. Xiaozhi Yang of Nanjing University and Prof. Lidong Dai of CAS Institute of Geochemistry improved the manuscript. This work was supported by the National Natural Science Foundation of China (Grant Nos. 41402041 & 41322015) and the Fundamental Research Funds for the Central Universities of China.*

References

Anderson D L, Sammis C G. 1970. Partial melting in the upper mantle. Phys Earth Planet Inter, 3: 41–50

Bagdassarov N S, Maumus J, Poe B, Slutskiy A B, Bulatov V K. 2004. Pressure dependence of Tg in silicate glasses from electrical impedance measurements. Phys Chem Glasses, 45: 197–214

Barnes H. 2015. Hydrothermal processes. Geochem Perspect, 4: 1–93

Blank J G. 1993. An experimental investigation of the behavior of carbon dioxide in rhyolitic melt. Doctoral Dissertation. Pasadena: California Institute of Technology

Caldwell W B, Klemperer S L, Rai S S, Lawrence J F. 2009. Partial melt in the upper-middle crust of northwest Himalaya revealed by Rayleigh wave dispersion. Tectonophysics, 477: 58–65

Chen L, Booker J R, Jones A G, Wu N, Unsworth M J, Wei W, Tan H. 1996. Electrically conductive crust in Southern Tibet from INDEPTH magnetotelluric surveying. Science, 274: 1694–1696

Coggon J A, Luguet A, Nowell G M. 2013. Hadean mantle melting recorded by southwest Greenland chromitite ^{186}Os signatures. Nature Geosci, 6: 871–874

Dingwell D B, Webb S L. 1990. Relaxation in silicate melts. Eur J Mineral, 2: 427–449

Dziewonski A M, Anderson D L. 1981. Preliminary reference Earth model. Phys Earth Planet Inter, 25: 297–356

Elkins-Tanton L T. 2012. Magma oceans in the inner solar system. Annu Rev Earth Planet Sci, 40: 113–139

Evans R L, Hirth G, Baba K. 2005. Geophysical evidence from the MELT area for compositional controls on oceanic plates. Nature, 437: 249–252

Faul U H. 2001. Melt retention and segregation beneath mid-ocean ridges. Nature, 410: 920–923

Fogo J K, Benson S W, Copeland C S. 1954. The electrical conductivity of supercritical solutions of sodium chloride and water. J Chem Phys, 22: 212–216

Francheteau J, Jaupart C, Shen X, Kang W, Lee D, Bai J, Wei H, Deng H. 1984. High heat flow in Southern Tibet. Nature, 307: 32–36

Franck E U. 1956. Hochverdichteter Wasserdampf II. Ionerdisoziation von KCl in H_2O bis 750°C. Zelt Phys Chem, 8: 107–126

Franck E U, Savolainen E, Marshall W L. 1962. Electrical conductance cell assembly for use with aqueous solutions up to 800°C and 4000 bars. Rev Sci Instrum, 33: 115–117

Frantz J D, Marshall W L. 1982. Electrical conductances and ionization constants of calcium chloride and magnesium chloride in aqueous solutions at temperatures to 600°C and pressures to 4000 bars. Am J Sci, 282: 1666–1693

Frantz J D, Marshall W L. 1984. Electrical conductance and ionization constants of salts, acids, and bases in supercritical aqueous fluids: 1. Hydrochloric-acid from 100°C to 700°C and at pressures to 4000 bars. Am J Sci, 284: 651–667

Fuoss R M, Shedlovsky T. 1949. Extrapolation of conductance data for weak electrolytes. J Am Chem Soc, 71: 1496–1498

Gaillard F. 2004. Laboratory measurements of electrical conductivity of hydrous and dry silicic melts under pressure. Earth Planet Sci Lett, 218: 215–228

Gaillard F, Iacono-Marziano G. 2005. Electrical conductivity of magma in the course of crystallization controlled by their residual liquid composition. J Geophys Res, 110: B06204, doi: 10.1029/2004JB003282

Guo X, Zhang L, Behrens B, Ni H. 2016. Probing the status of felsic magma reservoirs: Constraints from the P-T-H_2O dependences of electrical conductivity of rhyolitic melt. Earth Planet Sci Lett, 433: 54–62

Hashim L, Gaillard F, Champallier R, Breton N L, Arbaret L, Scaillet B. 2013. Experimental assessment of the relationships between electrical resistivity, crustal melting and strain localization beneath the Himalayan-Tibetan Belt. Earth Planet Sci Lett, 373: 20–30

Harris N, Ayres M, Massey J. 1995. Geochemistry of granitic melts produced during the incongruent melting of muscovite: Implications for the extraction of Himalayan leucogranite magmas. J Geophys Res, 100: 15767–15777

Henderson P, Nolan J, Cunningham G C, Lowry R K. 1985. Structural controls and mechanisms of diffusion in natural silicate melts. Contrib Mineral Petrol, 89: 263–272

Ho P C, Palmer D A. 1997. Ion association of dilute aqueous potassium chloride and potassium hydroxide solutions to 600°C and 300 MPa determined by electrical conductance measurements. Geochim Cosmochim Acta, 61: 3027–2040

Hofmann A W. 1988. Chemical differentiation of the Earth: The relationship between mantle, continental crust, and oceanic crust. Earth Planet Sci Lett, 90: 297–314

Huebner J S, Dillenburg R G. 1995. Impedance spectra of hot, dry silicate minerals and rock: Qualitative interpretation of spectra. Am Mineral, 80: 46–64

Huebner J S, Voigt D E. 1988. Electrical conductivity of diopside: Evidence for oxygen vacancies. Am Mineral, 73: 1235–1254

Jambon A. 1982. Tracer diffusion in granitic melts: Experimental results for Na, K, Rb, Cs, Ca, Sr, Ba, Ce, Eu to 1300°C and a model of calculation. J Geophys Res, 87: 10797–10810

Karato S, Wang D. 2013. Electrical conductivity of minerals and rocks. In: Karato S, ed. Physics and Chemistry of the Deep Earth. New York: John Wiley & Sons Ltd. 145–182

Kind R, Ni J, Zhao W, Wu J, Yuan X, Zhao L, Sandvol E, Reese C, Nabelek J, Heam T. 1996. Evidence from earthquake data for a partially molten crustal layer in Southern Tibet. Science, 274: 1692–1694

Laumonier M, Gaillard F, Sifre D. 2015. The effect of pressure and water concentration on the electrical conductivity of dacitic melts: Implication for magnetotelluric imaging in subduction areas. Chem Geol, doi: 10.1016/j.chemgeo.2014.09.019

Law R D, Searle M P, Simpson R L. 2004. Strain, deformation temperatures and vorticity of flow at the top of the Greater Himalayan Slab, Everest Massif, Tibet. J Geol Soc London, 161: 305–320

Li S, Unsworth M J, Booker J R. 2003. Partial melt or aqueous fluids in the Tibetan crust: Constraints from INDEPTH magnetotelluric data. Geophys J Int, 153: 289–304

Liebscher A, Heinrich C A. 2007. Fluid-fluid interactions in the earth's lithosphere. Rev Mineral Geochem, 65: 1–13
Liebscher A. 2010. Aqueous fluids at elevated pressure and temperature. Geofluids, 10: 3–19
Lowry R K, Henderson P, Nolan J. 1982. Tracer diffusion of some alkali, alkaline-earth and transition element ions in a basaltic and an andesitic melt, and the implications concerning melt structure. Contrib Mineral Petrol, 80: 254–261
McGary R S, Evans R L, Wannamaker P E. 2014. Pathway from subducting slab to surface for melt and fluids beneath Mount Rainier. Nature, 511: 338–340
Makovsky Y, Klemperer S L. 1999. Measuring the seismic properties of Tibetan bright spots: Free aqueous fluid in the Tibetan middle crust. J Geophys Res, 104: 10795–10825
Manning C E. 2004. The chemistry of subduction-zone fluids. Earth Planet Sci Lett, 223: 1–16
Marshall W L, Frantz J D. 1987. Electrical conductance measurements of dilute, aqueous electrolytes at temperatures to 800°C and pressures to 4000 bars: Techniques and interpretations. In: Ulmer G, Bames H L, eds. Hydrothermal Experimental Techniques. New York: John Wiley. 261–392
Murase T, McBirney A R. 1973. Properties of some common igneous rocks and their melts at high temperatures. Geol Soc Am Bull, 84: 3563–3592
Naif S, Key K, Constable S, Evans R L. 2013. Melt-rich channel observed at the lithosphere-asthenosphere boundary. Nature, 495: 356–359
Ni H, Hui H, Steinle-Neumann G. 2015. Transport properties of silicate melts. Rev Geophys, 53: 715–744
Ni H, Chen Q, Keppler H. 2014. Electrical conductivity measurements of aqueous fluids under pressure with a hydrothermal diamond anvil cell. Rev Sci Instrum, 85: 115107
Ni H, Keppler H. 2013. Carbon in silicate melts. Rev Mineral Geochem, 75: 251–287
Ni H, Keppler H, Manthilake M A G M. 2011a. Electrical conductivity of dry and hydrous $NaAlSi_3O_8$ glasses and liquids at high pressures. Contrib Mineral Petrol, 162: 501–513
Ni H, Keppler H, Behrens H. 2011b. Electrical conductivity of hydrous basaltic melts: Implications for partial melting in the upper mantle. Contrib Mineral Petrol, 162: 637–650
Noyes A. 1907. The Electrical Conductivity of Aqueous Solutions. Publication No. 63. Washington DC: Carnegie Institution of Washington
Poe B T, Romano C, Varchi V, Misiti V, Scarlato P. 2008. Electrical conductivity of a phonotephrite from Mt. Vesuvius: The importance of chemical composition on the electrical conductivity of silicate melts. Chem Geol, 256: 193–202
Pommier A, Gaillard F, Pichavant M, et al. 2008. Laboratory measurements of electrical conductivities of hydrous and dry Mount Vesuvius melts under pressure. J Geophys Res, 113: B05205, doi: 10.1029/2007JB005269
Pommier A, Gaillard F, Pichavant M. 2010a. Time-dependent changes of the electrical conductivity of basaltic melts with redox state. Geochim Comochim Acta, 74: 1653–1671
Pommier A, Gaillard F, Malki M, Pichavant M. 2010b. Methodological re-evaluation of the electrical conductivity of silicate melts. Am Mineral, 95: 284–291
Pommier A, Le-Trong E. 2011. "SIGMELTS": A web portal for electrical conductivity calculations in geosciences. Comput Geosci, 37: 1450–1459
Pommier A. 2014. Interpretation of magnetotelluric results using laboratory measurements. Surv Geophys, 1: 41–84
Presnall D C, Simmons C L, Porath H. 1972. Changes in electrical conductivity of a synthetic basalt during melting. J Geophys Res, 77: 5665–5672
Quist A S, Marshall W L. 1968. Electrical conductances of aqueous sodium chloride solutions from 0 to 800°C and at pressures to 4000 bars. J Phys Chem, 72: 684–703
Quist A S, Marshall W L. 1969. The electrical conductances of some alkali metal halides in aqueous solutions from 0 to 800°C and at pressures to 4000 bars. J Phys Chem, 73: 978–985
Quist A S, Marshall W L, Franck E U. 1970. Reference solution for electrical conductance measurements to 800°C and 12000 bars. Aqueous 0.01 demal potassium chloride. J Phys Chem, 74: 2241–2243
Rai C S, Manghnani M H. 1978. Electrical conductivity of ultramafic rocks to 1820 K. Phys Earth Planet Inter, 17: 6–13
Robb L. 2005. Introduction to ore-forming processes. Malden, MA, USA: Blackwell. 384
Royden L H, Burchfield B C, van der Hilst R D. 2008. The geological evolution of the Tibetan Plateau. Science, 321: 1054–1058
Rubie D C, Frost D J, Mann U. 2011. Heterogeneous accretion, composition and core-mantle differentiation of the earth. Earth Planet Sci Lett, 301: 31–42
Satherley J, Smedley S I. 1985. The electrical conductivity of some hydrous and anhydrous molten silicates as a function of temperature and pressure. Geochim Cosmochim Acta, 49: 769–777
Searle M P, Law R D, Jessup M. 2006. Crustal structure, restoration and evolution of the Greater Himalayan Nepal-South Tibet: Implications for channel flow and ductile extrusion of the middle crust. In: Law R D, Searle M P, Godin L, eds. Channel Flow, Ductile Extrusion and Exhumation in Continental Collision Zones. London: Geological Society London Special Publication. 355–378
Sharygin A V, Grafton B K, Xiao C, Wood R H, Balashov V N. 2006. Dissociation constants and speciation in aqueous Li_2SO_4 and K_2SO_4 from measurements of electrical conductance to 673 K and 29 MPa. Geochim Cosmochim Acta, 70: 5169–5182
Sifre D, Gardes E, Massuyeau M. 2014. Electrical conductivity during incipient melting in the oceanic low-velocity zone. Nature, 509: 81–85
Sifre D, Hashim L, Gaillard F. 2015. Effects of temperature, pressure and chemical compositions on the electrical conductivity of carbonated melts and its relationship with viscosity. Chem Geol, doi: 10.1016/j.chemgeo.2014.09.022
Sigmundsson F. 2006. Plate tectonics: Magma does the splits. Nature, 442: 251–252
Stern R J. 2002. Subduction zones. Rev Geophys, 40: 31–38
Su G L, Xie H S, Li H P, Guo J, Ding D Y. 2000. Determination of mean molar activity coefficients of electrolytes in aqueous solutions at high temperature and pressure. Bull Mineral Petrol Geochem, 19: 25–29
Sun W, Teng F, Niu Y, Tatsumi Y, Yang X. 2014. The subduction factory: Geochemical perspectives. Geochim Cosmochim Acta, 143: 1–7
Tyburczy J A, Waff H S. 1983. Electrical conductivity of molten basalt and andesite to 25 kilobars pressure: Geographical significance and implications for charge transport and melt structure. J Geophys Res, 88: 2413–2430
Tyburczy J A, Waff H S. 1985. High pressure electrical conductivity in naturally occurring silicate liquids. In: Schock R N, ed. Point Defects in Minerals. Washington DC: American Geophysical Union
Unsworth M J, Jones A G, Wei W, Project INDEPTH Team. 2005. Crustal rheology of the Himalaya and southern Tibet inferred from magnetotelluric data. Nature, 438: 78–81
Van Ngoc P, Boyer P, Therme P. 1986. Partial melting zones in the crust of Southern Tibet from magnetotelluric results. Nature, 319: 310–314
Waff H S, Weill D F. 1975. Electrical conductivity of magmatic liquids: Effects of temperature, oxygen fugacity and composition. Earth Planet Sci Lett, 28: 254–260
Wagner W, Pruss A. 2002. The IAPWS formulation 1995 for the thermodynamic properties of ordinary water substance for general and scientific use. J Phys Chem Ref Data, 31: 387–535
Watson E B. 1981. Diffusion in magmas at depth in the Earth: The effects of pressure and dissolved H_2O. Earth Planet Sci Lett, 52: 291–301
Wei W, Unsworth M, Jones A. 2001. Detection of widespread fluids in the Tibetan Crust by magnetotelluric studies. Science, 292: 716–718
Wyllie P J. 1988. Magma genesis, plate-tectonics, and chemical differentiation of the Earth. Rev Geophys, 26: 370–404
Xu Y S, Xie H S, Guo J, Zheng H F, Zhang Y M, Song M S. 1997. Conductivity of NaCl solution at 0.4–5.0 GPa and 25–500°C. Sci China Ser D-Earth Sci, 40: 398–402
Xu Z Q, Yang J S, Li H B, Zhang J X, Zeng L S, Jiang M. 2006. The Qinghai-Tibet Plateau and continental dynamics: A review on terrain tectonics, collisional orogenesis, and processes and mechanisms. Geol

China, 33: 221–238
Yang X. 2011. Origin of high electrical conductivity in the lower continental crust: A review. Surv Geophys, 32: 875–903
Yin A, Harrison T M. 2000. Geologic evolution of the Himalayan-Tibetan orogen. Annu Rev Earth Planet Sci, 28: 211–280
Yoshino T, Katsura T. 2013. Electrical conductivity of mantle minerals: Role of water in conductivity anomalies. Annu Rev Earth Planet Sci, 41: 605–628
Yoshino T, Matsuzaki T, Yamashita S. 2006. Hydrous olivine unable to account for conductivity anomaly at the top of the asthenosphere. Nature, 443: 973–976
Zheng H F, Xie H S, Xu Y S, Song M S, Guo J, Zhang Y M. 1997. Study on the electrical conductance of 0.025 mol NaCl solution at 0.25–3.75 GPa and 20–370°C. Acta Geol Sin, 71: 274–280
Zheng Y F, Hermann J. 2014. Geochemistry of continental subduction-zone fluids. Earth Planets Space, 66: 93
Zimmerman G H, Gruszkiewicz M S, Wood R H. 1995. New Apparatus for Conductance Measurements at High Temperatures: Conductance of Aqueous Solutions of LiCl, NaCl, NaBr, and CsBr at 28 MPa and Water Densities from 700 to 260 kg/m^3. J Phys Chem, 99: 11612–11625